Monte Carlo uncertainty of the ^{3}He$(\alpha,\gamma)^7$Be reaction rate

R. J. deBoer,* J. Görres, K. Smith, E. Uberseder, and M. Wiescher
The Joint Institute for Nuclear Astrophysics, Department of Physics, University of Notre Dame, Notre Dame, Indiana 46556, USA

A. Kontos
The Joint Institute for Nuclear Astrophysics, National Superconducting Cyclotron Laboratory, Michigan State University, East Lansing, Michigan 48823, USA

G. Imbriani and A. Di Leva
Università degli Studi di Napoli "Federico II" and INFN, Napoli, Italy

F. Strieder
Institut für Experimentalphysik, Ruhr-Universität Bochum, Bochum, Germany
(Received 11 March 2014; revised manuscript received 8 August 2014; published 19 September 2014)

Background: The ^{3}He$(\alpha,\gamma)^7$Be reaction is of critical importance in determining the flux of solar neutrinos through the *pp*-II and *pp*-III chains. For this reason and others, the description of the cross section and its extrapolation towards low-energy has always been a matter of intense debate. While large systematic differences have been present in the past, several recent measurements are all in excellent statistical agreement.
Purpose: The convergence of the recent individual experimental measurements of the ^{3}He$(\alpha,\gamma)^7$Be reaction prompts a global analysis of the reaction data. From the combined data, a more precise estimate of the low-energy cross section can be determined.
Results: A global R-matrix fit is used to describe the ^{3}He$(\alpha,\gamma)^7$Be data as well as scattering data over a similar energy range. The R-matrix fit is then subjected to a Monte Carlo analysis to extract the uncertainties on the cross section and corresponding reaction rate.
Conclusion: By combining several recent measurements of the ^{3}He$(\alpha,\gamma)^7$Be reaction, the combined data yield a zero energy S factor of $S(0) = 0.542 \pm 0.011$(MC fit) $\pm$ 0.006(model)$^{+0.019}_{-0.011}$(phase shifts) keV b. This gives a total uncertainty in $S(0)$ of $+0.023/-0.017$ keV b.

DOI: 10.1103/PhysRevC.90.035804 PACS number(s): 26.20.Cd, 26.35.+c, 26.65.+t, 27.20.+n

I. INTRODUCTION

The reaction ^{3}He$(\alpha,\gamma)^7$Be has been intensely studied over the last decades because of its critical role in the production of ^{7}Be during *pp*-chain hydrogen burning in low mass stars like our sun. By way of the *pp*-II chain, solar neutrinos are produced by electron capture on ^{7}Be. In the *pp*-III chain, proton capture occurs instead on ^{7}Be creating ^{8}B which subsequently β-decays [1].

Recent measurements of the fluxes of the ^{7}Be and ^{8}B solar neutrinos by the Borexino and SNO Collaborations have been made with a total uncertainty of less than 5% [2,3]. However, the total uncertainties of the corresponding flux calculations by means of the so-called standard solar model (SSM), considering the individual input parameter uncertainties, are larger, i.e., 6.2% and 12.5%[1] for the ^{7}Be and ^{8}B fluxes, respectively [4].

In order to continue to test solar model calculations against the observed ^{7}Be and ^{8}B solar neutrino fluxes, the level of uncertainty of all input parameters must be reduced. Among other parameters with presently large uncertainties, e.g., the ^{7}Be$(p,\gamma)^8$B cross section and the opacity, this holds in particular for the ^{3}He$(\alpha,\gamma)^7$Be cross section at solar temperature. The present uncertainty of 5% [1] is the largest contribution to the ^{7}Be flux uncertainty and a major contribution for the ^{8}B flux uncertainty (see Table III of Ref. [4]). A substantial reduction would directly translate into a reduction of the SSM calculation uncertainties and will have important consequences for the interpretation of solar neutrino experiments.

In recent years, independent measurements of the ^{3}He$(\alpha,\gamma)^7$Be cross section have yielded remarkably consistent results. This includes results from both activation and prompt γ ray detection methods. This is in contrast to the "classic" measurements [5–12] (see Fig. 1) as summarized in Ref. [12]. In Ref. [13] it was demonstrated that the "recent" data [13–18] could all be described consistently by a multichannel R-matrix fit. This includes the low-energy data measured at the laboratory for underground nuclear astrophysics (LUNA) presented in Ref. [15] (originally in Refs. [19,20]) and the higher energy data from the European recoil separator for nuclear astrophysics (ERNA) given in Ref. [17]. In the intermediate energy region, measurements with very low systematic and statistical uncertainties have been reported [14,16,18]. In the interim, new measurements have been made at the Institute of Nuclear Research of the Hungarian Academy

*rdeboer1@nd.edu

[1]Rounding errors resulted in an overestimate of the reaction rate uncertainty quoted in Ref. [4]. A value of 5% has been adopted when quoting the rate from Ref. [1]. This correction has been applied to the total flux estimates given here.

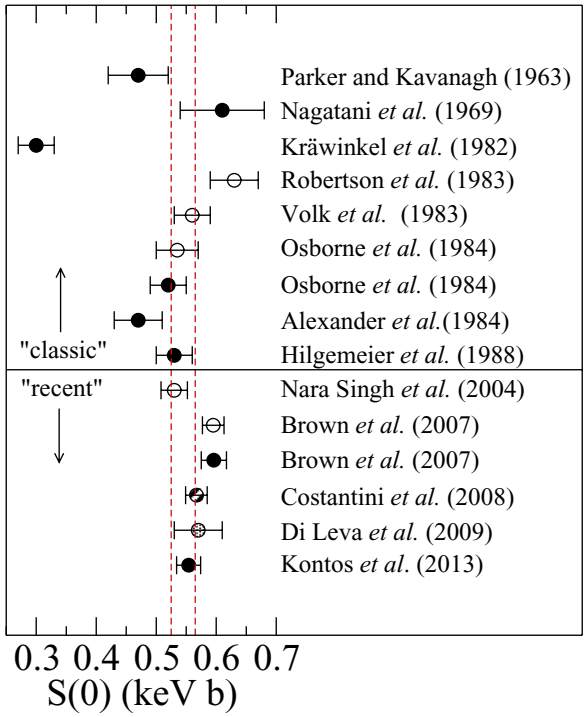

FIG. 1. (Color online) Summary of previous extrapolations of the ^{3}He$(\alpha,\gamma)^7$Be S factor to zero energy. The solid central line is the demarcation between recent and classic measurements. The closed circle points signify measurements made using prompt γ rays, the open circles using activation. The crossed circle for Ref. [15] represents an extrapolation made with both prompt and activation data. The mesh pattern point of Ref. [17] signifies a recoil separator measurement. Note that while the measurement of Ref. [13] was of prompt γ rays, the extrapolation used all of the recent data. The vertical red dashed lines indicate the 68% confidence region determined by combining the recent data using an R-matrix framework and a Monte Carlo uncertainty analysis. There are no values given for Refs. [18,21] because an extrapolation was not made in those works. Note that the outlying value of Ref. [7] is due to mistakes in the data analysis as discussed in Ref. [12].

of Sciences (ATOMKI) [21] which are also consistent with the previous analysis.

It should be noted that while the earlier measurements yielded somewhat different cross sections than those found recently, this difference is likely not one of experimental error but reflects the complexity of the measurement and analysis. The discrepancies between older data and the more recent measurements are often the result of better known stopping powers, the ability to perform more precise geometric corrections, and efficiency determinations. It may be possible to correct for these effects if enough experimental information is provided, but this is beyond the scope of the current work.

From previous experimental measurements, when the uncertainties on the cross section measurements were much larger, the external capture model was sufficient to reproduce the trend of the data [5,22]. But recent experimental results, because of their increased precision and extension to higher energies, show significant deviations from the external capture model, prompting a need for the inclusion of an internal component [23–25]. Using the R-matrix method [26], the large $E1$ capture cross section at low energy can be reproduced by combining $E1$ external and internal s-wave capture contributions. The external part comes from the traditional external capture model [27–30], the internal part primarily from a $J^\pi = 1/2^+$ background pole which includes the channel capture contribution. The interference between the internal and external contributions is found to be critical in reproducing the magnitude of the cross section while the inclusion of channel capture influences the low-energy shape.

In this work the R-matrix analysis of Ref. [13] is continued. An updated analysis is presented and the final result is subjected to a Monte Carlo uncertainty method. By combining the statistically consistent results of the recent ^{3}He$(\alpha,\gamma)^7$Be cross section measurements, a more confident estimate of the reaction rate can be obtained. In Sec. II, a detailed review of the R-matrix calculation is given. This is followed by a general description of the Monte Carlo technique in Sec. III which quantifies the combined experimental uncertainties, and Sec. IV where the R-matrix model uncertainties are characterized. In Sec. V the systematic uncertainty from the choice of scattering data used to obtain the phase shifts is addressed. Reaction rates and their total uncertainties are then presented in Sec. VI. Concluding remarks are given in Sec. VII.

II. *R*-MATRIX ANALYSIS

The capture cross section for ^{3}He$(\alpha,\gamma)^7$Be is described using R-matrix theory [26] and implemented using the code AZURE2 [31,32]. The formalism uses first order perturbation theory to include resonant γ-ray exit channels in the standard nonrelativistic R-matrix of Ref. [26] and uses the methods described in Refs. [28–30] to include the radiative capture contributions using the external capture model and background poles which include their channel capture contributions. The alternate parametrization presented in Ref. [33] is utilized. A channel radius of 4.3 fm is used and the sensitivity of the fit to this model parameter is further explored. The data under investigation cover an energy range from the α particle separation energy [$S_\alpha = 1.5866(5)$ MeV] up to nearly the proton separation energy [$S_p = 5.6058(7)$ MeV, $E_{\rm cm} = 3.5$ MeV] in the ^{7}Be compound nucleus (see Fig. 2 and Table I). While the background pole energies are placed at 11 MeV, this placement is somewhat arbitrary. Background pole energies were tested up to 30 MeV and the same quality fits could be obtained. The deviation in the extrapolated S factor due to choice of channel radius and pole energy is detailed in Sec. III.

In the model, the reduced γ widths (γ_γ) have contributions from the internal and external regions (see, e.g., Ref. [28]) where $\gamma_\gamma = \gamma_{\rm int} + \gamma_{\rm ext}$. Here $\gamma_{\rm int}$ is the contribution to the γ width from the internal (resonance) region ($r < r_c$) and $\gamma_{\rm ext}$ is the contribution from the external (channel) region ($r > r_c$). This modification of the γ width by the external component modifies the magnitude and energy dependence of the background pole contribution to the cross section. As an example, a comparison of the background pole contribution for the ground state transition with and without channel capture is given in Fig. 3.

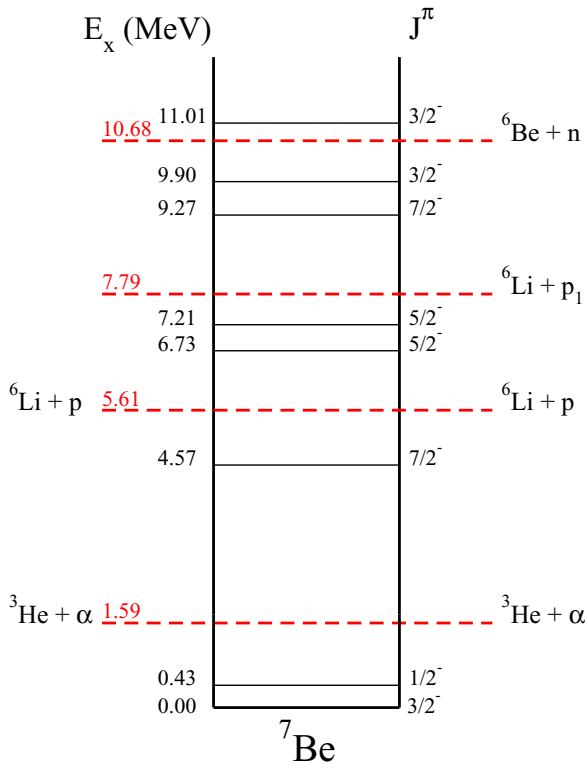

FIG. 2. (Color online) Level diagram of ^{7}Be. The low-mass nucleus has only two bound states: the ground state and the level at $E_x = 0.429$ MeV. It may be noted that no capture measurements have been made above the proton separation energy.

The total capture cross section is the sum of the decays to the ground state and first excited state in ^{7}Be, the only two bound states (see Fig. 2). Cross sections from each transition have been fit, defining the branching ratio as a function of energy. The total cross section is fit where the individual transitions are not available. Currently, the highest energy experimental data for the ^{3}He$(\alpha,\gamma)^7$Be reaction data terminates just below the proton separation energy at $S_p = 5.61$ MeV [17]. For this reason, the analysis is limited to the α particle and γ ray channels.

The different R-matrix components used to reproduce the observed ^{3}He$(\alpha,\gamma)^7$Be cross section data are shown in Fig. 4.

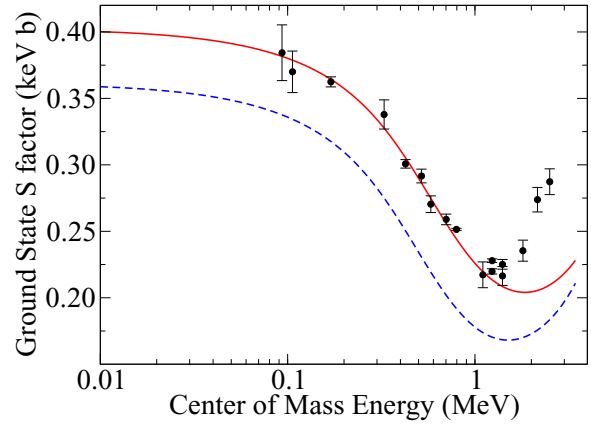

FIG. 3. (Color online) A comparison of R-matrix calculations of the angle integrated cross section for the ground state transition of the ^{3}He$(\alpha,\gamma)^7$Be reaction. The lines show calculations of the $E1$ external capture plus the $E1$ contribution from a $1/2^+$ background pole. The solid red line is an R-matrix calculation with channel capture, the dashed blue line represents a calculation where the channel capture is neglected. Ground state transition data from Refs. [15–17] subjected to the normalizations given in Table I are shown for comparison.

The $E1$ s-wave external capture produces the most significant contribution at low energies, but cannot solely reproduce the magnitude and shape of the experimental data. An additional background pole contribution, while by itself a rather small contribution to the total cross section at low energy, can interfere constructively with the external capture to reproduce both the magnitude and shape of the experimental data. This is a clear example of where a much smaller contribution to the cross section can have a significant effect by way of the interference between two components, which is proportional to $2\sqrt{\sigma_1\sigma_2}$ (see, e.g., Appendix A.3 of Ref. [35]). The background pole which is most significant is a $1/2^+$ (s-wave, $E1$). At higher energy, above $\sim$1 MeV, d-wave $E1$ contributions, mainly from a $3/2^+$ background pole, are needed to reproduce the capture cross section.

A single resonance ($J^\pi = 7/2^-$) is present at $E_{\rm cm} = 3.0$ MeV ($E_x = 4.6$ MeV) which makes a small contribution as observed in the data of Ref. [17]. The $7/2^-$ resonance is also prominent in the scattering data providing additional constraint

TABLE I. Data sets considered in the the present analysis. The quoted systematic uncertainty is also given. The normalization is the result of the R-matrix fit using a χ^2 measure of the goodness of fit.

Data set	N	$E_{\rm cm}$ (MeV)	Transition	Syst. unc.	Norm.	χ^2/N
Barnard *et al.* (Elastic) [34]	593	1.4–3.2	G.S.	5%	1.017	0.77
Singh *et al.* (2004) (Activation) [14]	4	0.42–0.95	Total	3.7%	1.055	0.54
Costantini *et al.* (2008) (Activation) [15]	6	0.09–0.17	Total	3.2%	1.008	0.88
Costantini *et al.* (2008) (Prompt) [15]	3,3	0.09–0.17	G.S., 1st E.S.	3.8%	0.991	0.27,0.34
Brown *et al.* (2007) (Activation) [16]	8	0.33–1.23	Total	3.0%	0.973	2.48
Brown *et al.* (2007) (Prompt) [16]	8,8	0.33–1.23	G.S., 1st E.S.	3.5%	0.972	2.17,2.61
Di Leva *et al.* (2009) (Activation) [17]	48	0.70–3.13	Total	5.0%	0.972	0.79
Carmona-Gallardo *et al.* (2012) (Activation) [18]	3	1.05–2.80	Total	3.0%	0.965	0.52
Kontos *et al.* (2013) (Prompt) [13]	17	0.30–1.45	Total	8.0%	0.965	0.65
Bordeanu *et al.* (2013) (Activation) [21]	5	1.5–2.5	Total	6.0%	1.004	0.90

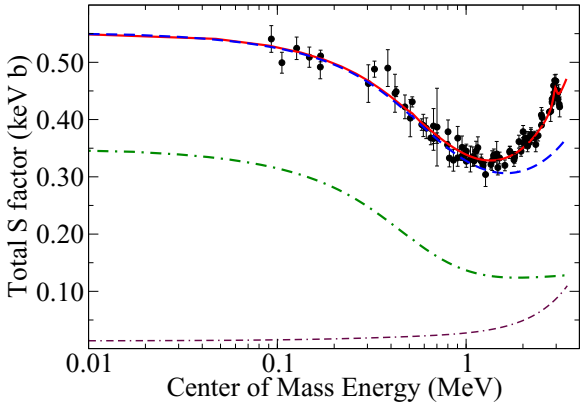

FIG. 4. (Color online) Different R-matrix components used for the fit to the ^{3}He$(\alpha,\gamma)^7$Be cross section. The data points are all recent data from Refs. [13,15–18,21]. The red solid line represents the best fit to the data which is similar to that previously given in Ref. [13]. The blue dashed line is the contribution from the s-wave $E1$ external capture and background pole ($J^\pi = 1/2^+$). The dot-dashed green line represents the pure external capture contribution. The maroon dash-dash-dotted line represents purely the $1/2^+$ background pole contribution. The plot illustrates the importance of the interference term between the background pole and the external capture. While the background pole contribution is itself small, the interference term is proportional to $2\sqrt{\sigma_{\rm BGP}\sigma_{\rm EC}}$. All contributions are the sum of the ground state and first excited state decays.

on its α width and energy. It is assumed that the contribution to the total capture cross section data is purely the result of $E2$ deexcitation to the ground state, as an $M3$ multipolarity would be required for a decay to the first excited state. The simultaneous fit of the scattering data of Ref. [34] and the capture data of Ref. [17] provides a more constrained value of $\Gamma_{\gamma_0} = 46(15)$ meV over that presented in Ref. [17] where only the capture data were considered. The α width of this state is listed in the compilation as $\Gamma_\alpha = 175(7)$ keV [36] which is in agreement with the value of 150(20) keV found here (see Table II).

For the scattering data, several background pole contributions were found to be necessary, as detailed in Ref. [13], as a deviation from purely hard sphere scattering is evident. These contributions are quite large, in several cases exceeding their Wigner limits (see Table II). These large values seem reasonable considering that the poles are accounting for the total widths of the higher energy single-particle resonances which have substantial branchings (see, e.g., Refs. [22,37,38]) into other particle channels as they open (see Fig. 2). A similar situation has been observed in the ^{12}C$(\alpha,\alpha)^{12}$C data (e.g. Ref. [39]) where the ^{16}O compound nucleus likewise has many observed single-particle states.

The R-matrix fit uses the χ^2 method as a measure of the goodness of the fit. The contributions to the total χ^2 come from both the difference of the individual data points from the R-matrix calculation and an additional term for the normalization factor of each data set [40]. The additional term in the total χ^2 calculation for the normalizations is critical in this uncertainty analysis where the systematic uncertainties dominate. There are also common uncertainties that are present between prompt and activation techniques for the same experiment. These common uncertainties are included using the method described by Ref. [41] as given in Eq. (5) of that work.

Table I summarizes the data which are considered and the normalizations resulting from the R-matrix fit. The analysis combines the results from several different ^{3}He$(\alpha,\gamma)^7$Be measurements. The results are very similar to those given in Ref. [13] but have slight differences because of some changes in the data and the inclusion of common uncertainties in the data of Refs. [15,16]. Table II gives the level parameters used for the R-matrix fit including the internal and external reduced widths of the γ ray decays.

There are two changes to the capture data compared to those given in Ref. [13]. The first is the exclusion of the prompt γ-ray and activation data of Ref. [17]. This has been done because some common uncertainties exist between the prompt, activation, and recoil data sets which could not be separated using the current uncertainty analysis method. The choice has been made to retain only the recoil data since they contain the majority of the experimental measurements. The second change is a modification to the over all normalization of the data of Ref. [14]. For the branching ratio of the decay of ^{7}Be

TABLE II. R-matrix best fit parameters ($r_c = 4.3$ fm). The fit used 16 free parameters which are displayed in **bold**. All other parameters were fixed. The sign of the partial widths indicates the sign of the interference. For comparison with the α widths of the background poles, the Wigner limits are given.

E_x	J^π	l	Γ_W[a] (MeV)	Γ_α (MeV)	$\Gamma_\gamma(0)$ (keV)	$\gamma_{\rm int}+\gamma_{\rm ext}(0)$ (MeV$^{1/2}$)	$\Gamma_\gamma(429)$ (keV)	$\gamma_{\rm int}+\gamma_{\rm ext}(429)$ (MeV$^{1/2}$)
11	$1/2^+$	0	9.4	**19.3**	**−0.79**	$-1.29-(0.17+i0.41)$	**0.13**	$0.41+(0.13+i0.41)$
11	$1/2^-$	1	8.7	**12.1**				
11	$3/2^+$	2	7.2	**11.1**	**0.24**	$-0.78-(0.06+i0.12)$	**0.34**	$-0.88-(0.16+i0.32)$
11	$3/2^-$	1	8.7	**12.0**				
11	$5/2^+$	2	7.2	**11.1**				
7	$5/2^-$	3	1.9	**2.9**				
4.56	$7/2^-$	3	0.36	**0.15**	**46**$\times10^{-6}$	$1.29+(0.73+i0.28)$		
11	$7/2^-$	3	5.0	**8.8**				
ANC(0) = **3.7** fm$^{-1/2}$						ANC(429) = **3.6** fm$^{-1/2}$		

[a]Γ_W is the α width derived from the Wigner limit, calculated from the equation $\Gamma_W = 2P\gamma_W^2$, where P is the penetrability and $\gamma_W^2 = (3/2)\hbar^2/(\mu r_c^2)$.

to the $E_x = 478$ keV state in ^{7}Li, Ref. [14] used a value of 10.44%. The remaining data sets considered in this analysis use an updated value of 10.52% [36]. This updated branching has been applied to the data of Ref. [14] resulting in an increase in the overall normalization of the data of 0.77%.

The dependence of the fit on the low-energy LUNA [19,20] data have also been tested. While the LUNA data reach much lower in energy than any other measurements, the upper energy limit of the Gran Sasso 400 kV accelerator also prevents overlap with other higher energy measurements. Performing the fit without the LUNA data shows a maximum deviation in the S factor from the fit with all data included of <1%. This shows that the low-energy energy dependence is driven by the higher energy data and the constraints of the R-matrix model.

Of the normalization factors given in Ref. [13], only that of Ref. [14] is outside the quoted systematic uncertainty. If this data set is neglected in the fit, the R-matrix cross section increases by about 1% over the entire energy range of the data.

Table I lists the reduced χ^2 of each of the data sets resulting from the fit. In general, the fit to each of the ^{3}He$(\alpha,\gamma)^7$Be data sets results in a reduced χ^2 which is close to one. This is in part because most of the data sets have very similar energy dependence. The only outlying data set is that of Ref. [16]. Here the three lowest energy data points in the total cross section activation data trend higher in cross section than the other data sets and the R-matrix fit. The prompt data are in much better agreement with the other data and the R-matrix fit with their larger reduced χ^2 coming from the large disagreement in the two highest energy data points.

A measure for the probability that the model under consideration is a reasonable representation of the data can be given by a p value test (see, e.g., Refs. [42,43]). For a χ^2 test, the probability function is the incomplete gamma function $Q(\nu,\chi^2)$. Here ν is the number of degrees of freedom, i.e., the number of data points minus the number of fit parameters. For the best fit, taking both the scattering and the capture data, the resulting p value is $Q(706-16,579) = 0.999$. This value is a result of the excellent fit to the scattering data and the large number of scattering data points. If the scattering data contribution is removed the p value is $Q(113-16,122.4) = 0.042$. The major contribution to the χ^2 now comes from the data of Ref. [16] (see Table I). If the scattering data and those of Ref. [16] are excluded a p value of $Q(89-16,64.3) = 0.76$ is obtained. The effects of the data of Ref. [16] on the uncertainty analysis are discussed in Sec. III.

III. MONTE CARLO UNCERTAINTY METHOD

From the global R-matrix fit, the combined uncertainty can be extracted using a frequentist Monte Carlo uncertainty method. A Baysian Monte Carlo method was recently performed in Ref. [41] but using a different model and fewer data sets. References [44,45] have used similar approaches for the reaction ^{12}C$(\alpha,\gamma)^{16}$O. In the following, the general approach is described as adapted from Ref. [42].

(i) The best fit from the R-matrix analysis is taken as the most probable description of the cross section. The minimization χ^2 method is used to define the goodness of the fit including normalization uncertainties and common uncertainties.

(ii) The data are subjected to a random variation. For each data point, the value from the R-matrix fit is assumed to be the most probable actual value of the cross section. The data are then resampled, assuming a Gaussian probability density function (PDF), around the best fit cross section value. The uncertainty on the data point is scaled by the square root of the ratio of the cross section of the fit to the cross section of the Gaussian randomized cross section.

(iii) The systematic normalization for each experimental data set is also resampled. These are randomly deter mined assuming a Gaussian distribution for the PDF.

(iv) The R-matrix fit is then performed again. The initial values of the parameters are purposely chosen to be rather far from their best fit values in an attempt to avoid a bias in the fitting.

(v) The process then repeats steps 2–4 many times (referred to as the "MC iterations"). In this case, a sample size of 5000 iterations has been chosen as a compromise between computation time and accuracy. For each of the MC iterations, an extrapolation of the cross section can be made using the best fit parameters from that iteration. This cross section is then numerically integrated to calculate the reaction rate at a given temperature.

The results of each of the MC iterations, for each quantity of interest, can then be represented by a histogram. The quantity of interest may be one of the fit parameters, the cross section at a particular energy, or the reaction rate at a particular temperature. The distribution of the histogram is then the PDF of the quantity of interest. The lower and upper uncertainties are then defined by the 16% and 84% quantiles of the histogram. The central value is defined as the 50% quantile. The PDF of the cross section at an example energy of $E_{\rm cm} = 12.9$ keV is shown in Fig. 5.

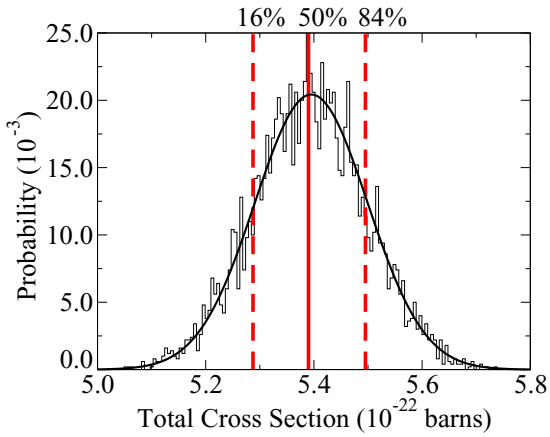

FIG. 5. (Color online) Probability density function of the ^{3}He$(\alpha,\gamma)^7$Be cross section at an example energy of $E_{\rm cm} = 12.9$ keV. The solid red line represents the 50% quantile, the red dashed lines represent the 16% and 84% quantiles. The black solid line is a Gaussian fit which matches the shape of the PDF.

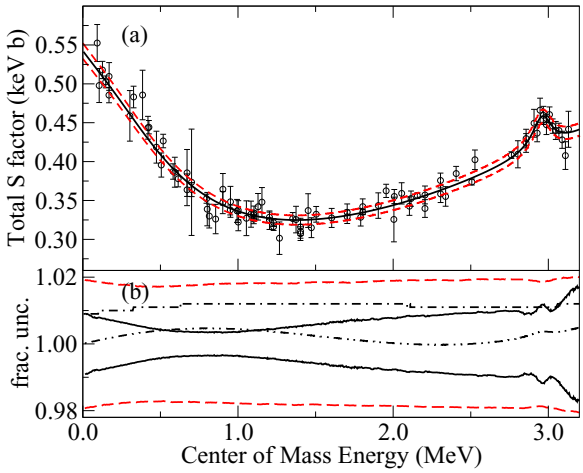

FIG. 6. (Color online) Uncertainties on the ^{3}He$(\alpha,\gamma)^7$Be S factor as determined by the Monte Carlo analysis. Panel (a) shows the uncertainty of the S factor. The black solid line represents the best fit while the dashed red lines represent the 16% and 84% uncertainty quantiles. The fractional uncertainty is shown in (b). The dashed red line represents the combined systematic and statistical uncertainties. The black solid line represents the statistical uncertainties alone. The black dotted-dashed line represents the deviation of the fit (fit without Ref. [14] data/fit with all data) if the data of Ref. [14] are excluded (see text). The black dot-dot-dashed line represents the deviation (fit without Ref. [15] data/fit with all data) of the fit without the LUNA data of Ref. [15].

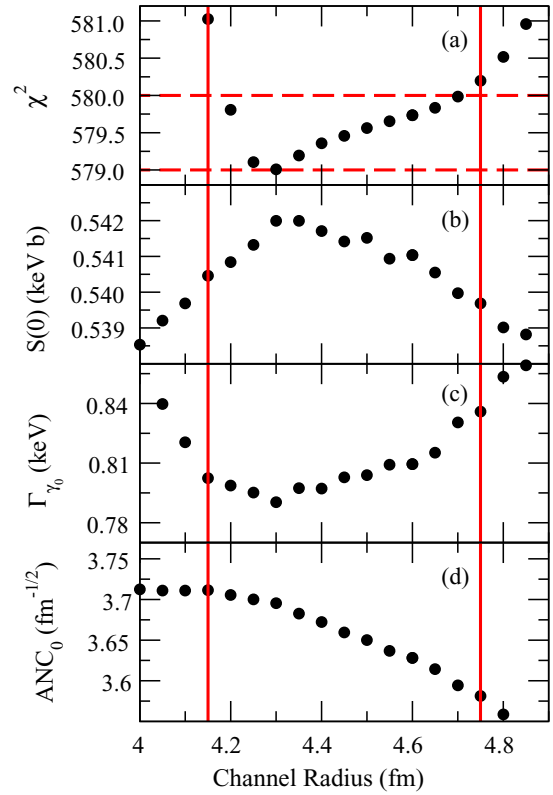

FIG. 7. (Color online) Sensitivity of the R-matrix fit as a function of channel radius. Panel (a) shows the sensitivity to the total χ^2, (b) the zero energy S factor, (c) the ground state γ width of the $1/2^+$ background pole, and (d) the ground state ANC. A change of $\Delta\chi^2 = 1$ is used to define the range of radius as shown by the dashed red lines in (a). An acceptable range of 4.15 fm $< r_{ch} <$ 4.75 fm is found which corresponds to an asymmetric variation in $S(0)$ of -0.002 keV b. This asymmetry causes a maximum in $S(0)$ which is a result of the interplay between the external capture contribution and the $1/2^+$ background pole as shown in (c) and (d).

As discussed in Sec. II, the data of Ref. [16] show a discrepancy with respect to the R-matrix fit, e.g., a large χ^2 (see Table I). There is no obvious reason for this, and subsequently the data of Ref. [16] were retained for the best fit. Nevertheless, to test the effect of these data on the uncertainty, the MC analysis was repeated with the data of Ref. [16] excluded. The result was almost negligible with a maximum increase in the uncertainty of 0.2% and a maximum difference in the central value of 0.1%.

The results of the Monte Carlo uncertainty analysis for the total capture cross section are shown in Fig. 6(a). The uncertainty over the range of the experimental data is ∼2.0%. The lack of resonance contributions to the cross section, except for the small contribution near $E_{\rm cm} = 3$ MeV, results in a particularly uniform uncertainty as highlighted in Fig. 6(b). Figure 6(b) also shows the effect that the data from Refs. [19,20] and Ref. [13] have on the fit as discussed in Sec. II. The central value of $S(0)$ is found to be 0.542 keV b and the uncertainty contribution from the MC analysis is ±0.011(MC fit) keV b.

IV. MODEL UNCERTAINTIES

The total uncertainty also includes systematic uncertainties from R-matrix model parameters. These are chiefly from the choice of background pole energies and channel radius. The fit is found to be insensitive to the choice of background pole energies to <1% when the background pole energies are varied between $E_x = 10$ and 30 MeV and the partial widths are then allowed to refit. The exception to this is the $J^\pi = 5/2^-$ background pole. While the χ^2 of the fit is still relatively insensitive to the energy of the pole (i.e., $\Delta\chi^2 < 1$), at increasing energies the α width becomes much larger than the Wigner limit. This is not unexpected since the pole must account for the effect of the two broad $5/2^-$ resonances reported in the compilation [36] at energies just above the proton separation energy (see Fig. 2) which are not included explicitly in the calculation. A 1% symmetric uncertainty is chosen as a conservative estimate over the range of the data.

To illustrate the sensitivity of the fit to the channel radius, the channel radius was varied as shown in Fig. 7 and compared to the change in χ^2 and the change in $S(0)$. The asymmetric behavior of $S(0)$, as shown in Fig. 7(b), is a result of the interplay between the external capture contributions, characterized by the asymptotic normalization coefficients (ANCs), and the background pole which has both internal and external contributions to its partial γ ray widths. As the radius changes the fit prefers a different ratio of external capture to background pole contribution. Figure 7(c) shows the ground state γ width of the $1/2^+$ background pole and Fig. 7(d) shows

the variation of the ground state ANC as a function of channel radius. The plot shows how the two values mirror each other as a function of channel radius.

To define an acceptable range for the channel radius model parameter, the radius was varied until a change in χ^2 of 1 was observed. The variation in χ^2 is shown in Fig. 7(a) and the corresponding change in $S(0)$ is shown in Fig. 7(b). The $S(0)$ reaches a maximum value at 4.3 fm, the same radius where the lowest χ^2 is observed. The range of channel radius is from $4.15 < r_c < 4.75$ fm and the variation of $S(0)$ is asymmetric, producing an uncertainty contribution of -0.002 keV b.

The contribution to the uncertainty in the S factor from the choice of background pole energies and choice of channel radius is taken as the two contributions summed in quadrature, $+1.0\%/-1.1\%$. This results in an uncertainty contribution for the zero energy S factor of $S(0) = 0.542 \pm 0.006$(model) keV b.

V. PHASE SHIFT UNCERTAINTY

As discussed in Sec. II, the data of Ref. [34] were chosen to define the phase shifts and their uncertainties in the R-matrix calculation. The choice of data set can cause a systematic bias in the extrapolation of the capture data that must be explored.

Several measurements of the scattering cross section are reported in the literature [37,46–52] but most lack detailed descriptions of their uncertainties. The data of Ref. [34] were found to contain the most uncertainty information and cover the most complete angular and energy range. The data were digitized from Fig. 2 of that work by the authors.[2] The statistical uncertainties are not given in the figure of Ref. [34], but the text states that they are about 3% with larger uncertainties in regions of low cross section. An additional systematic uncertainty of 5% is also present. The adopted point-to-point uncertainties are therefore taken as 3% except in regions of low cross section. Here the point size from the linear cross section plot is taken as the uncertainty when it exceeds 3%. The fit to the scattering data of Ref. [34], performed simultaneously with the capture data, is shown in Fig. 8.

Sensitivity tests were then performed by including other data sets in the analysis and what systematic uncertainties and statistical uncertainties were adopted. These ambiguities arise because the several of the studies lack experimental details on the uncertainties. From these sensitivity tests, several useful conclusions could be drawn. The precise value of the systematic uncertainties of the scattering data had little effect on the fits of the scattering data and on the uncertainties obtained by the MC analysis. Systematic uncertainties from 5% to 15% were investigated as well as completely removing the systematic uncertainty constraint. The $\Delta\chi^2$ method was again used as a judge of the reasonableness of the fits. The different values of the systematic uncertainties on the scattering data did not produce changes in the χ^2 which were significant compared to the value of $\Delta\chi^2 = 1$. Additionally, variations in the extrapolation to $S(0)$ were found to be $\sim$0.1% of the best fit value showing that the impact on the uncertainty was negligible.

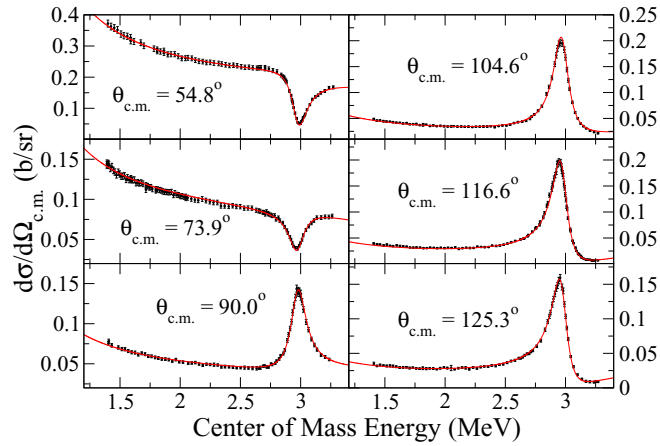

FIG. 8. (Color online) Example excitation curves representative of the fit to the ^{3}He(α,α)^{3}He data of Ref. [34] performed simultaneously with the capture data. The data have been digitized from Fig. 2 of that work by the authors.

The details of the point-to-point uncertainties proved to have a much more significant impact, producing large changes in χ^2. This uncertainty is a combination of the statistical uncertainties and additional varying systematic uncertainties. The two experimental measurements with small statistical uncertainties [46,50] had a large impact on the fit. While the statistical uncertainties of Ref. [46] are not available on EXFOR, they were obtained through private communication [54]. For both of these measurements, the error bars are often $<1\%$ but fluctuations in the values of nearby data points are much larger than the statistical errors. This indicates the presence of other sources of uncertainty which have not been considered. Fits to these data sets, with the statistical uncertainties only, resulted in large deviations in the χ^2 (i.e., $\chi^2/N \gg 1$) and the extrapolation of $S(0)$ ($>5\%$). This was the result of significant changes in the ANCs (3.0–5.5 fm$^{-1/2}$) and the background pole α widths. This was most significant for fits to the lowest energy scattering data of Ref. [46]. Since the scattering data were now a variable in the fitting, the change in χ^2 of the capture data alone was used as a basis for the comparison with the $\Delta\chi^2$ value.

Tests were then made by inflating the point-to-point uncertainties of the data sets so that the χ^2/N of each scatting data set was equal to 1. This, by construction, satisfies the $\Delta\chi^2$ condition but still produces variations in the fit reflective of the different scattering data sets. The range of different S factors obtained is shown in Fig. 9. The increased uncertainty at astrophysical energies due to the ambiguities in the low-energy scattering data is evident. This range of S factors is treated as an additional systematic uncertainty. It results in an additional uncertainty in $S(0)$ of $0.542^{+0.019}_{-0.011}$(phase shifts) keV b.

[2]A digitization of this data was also available on EXFOR [53]. It was found that this digitization had a significant offset in the energy scale of several of the excitation curves.

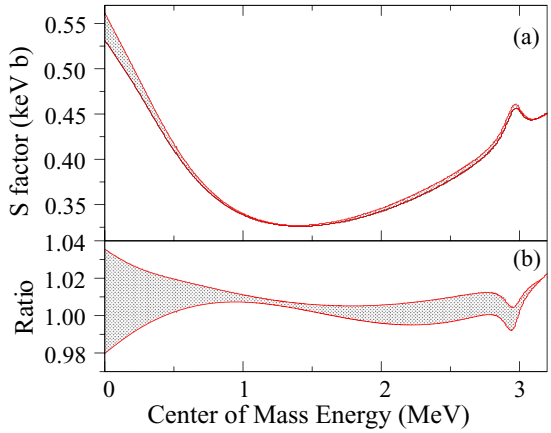

FIG. 9. (Color online) The shaded region in (a) represents the range of different S factors obtained from different combination of the scattering data sets from the literature [34,37,46–52]. The point-to-point uncertainties were inflated so that the χ^2/N of the scattering data sets was equal to 1. Panel (b) shows the ratio and the uncertainty with respect to the best fit using Ref. [34] as the only scattering data set.

VI. REACTION RATE UNCERTAINTY

The reaction rate uncertainty is calculated by numerical integration of the cross sections. The uncertainty from the Monte Carlo analysis is then summed in quadrature with the model uncertainty and the phase shift uncertainty. The reaction rate, with the overall uncertainty, is given in Table III. The central value of the rate differs somewhat from that presented in Ref. [13] because of the different data sets considered and the inclusion of common uncertainties. The total uncertainty is somewhat larger than that given in Ref. [13], despite the addition of another capture data set. The reason for this is the inclusion of the uncertainty contribution from the choice of scattering data sets which was previously neglected. Example PDFs for the MC portion of the reaction rate uncertainty are shown at representative temperatures of $T = 0.01$, 0.1, and 1 GK in Fig. 10.

It should also be noted that the rate at high temperature has significant contributions from the extrapolation of the R-matrix cross section to higher energies than the current data sets extend. Therefore, the rates are truncated at $T = 4$ GK where these contributions are estimated to be less than 1%.

Often a parametrization of the S factor energy dependence by means of a Taylor expansion of the S factor is performed [55]. Derivatives of $S(0)$ are then quoted instead of the numerical reaction rate. At $E_{\rm cm} < 0.5$ MeV the S factor is found to be well approximated by a linear function. The logarithmic derivative of the zero energy S factor is then found to be $S(0)'/S(0) = -0.50\ \mathrm{MeV}^{-1}$.

VII. CONCLUSION

As one of the most critical reactions for understanding the neutrino production in our sun through the pp-II and pp-III chains, the reaction rate for ^{3}He$(\alpha,\gamma)^7$Be is desired

TABLE III. Reaction rate for ^{3}He$(\alpha,\gamma)^7$Be. The central value of the rate is taken as the 50% quantile of the PDF resulting from the Monte Carlo analysis. The lower and upper uncertainties are found by summing in quadrature the 16% and 84% quantiles of the PDFs, respectively, with the model uncertainties. It should be noted that the highest temperature reaction rates require an extrapolation of the R-matrix cross section to higher energies than the current data extend. Therefore, the uncertainties quoted for these rates are likely underestimated.

T (GK)	$N_A\langle\sigma v\rangle$ (cm^3 mole^{-1} s^{-1})		
	Central value	Lower bound	Upper bound
0.005	5.076×10^{-25}	4.898×10^{-25}	5.287×10^{-25}
0.010	1.679×10^{-18}	1.627×10^{-18}	1.749×10^{-18}
0.011	1.014×10^{-17}	9.823×10^{-18}	1.056×10^{-17}
0.012	4.973×10^{-17}	4.820×10^{-17}	5.180×10^{-17}
0.013	2.060×10^{-16}	1.997×10^{-16}	2.146×10^{-16}
0.014	7.420×10^{-16}	7.192×10^{-16}	7.729×10^{-16}
0.015	2.376×10^{-15}	2.303×10^{-15}	2.474×10^{-15}
0.016	6.882×10^{-15}	6.672×10^{-15}	7.168×10^{-15}
0.018	4.513×10^{-14}	4.375×10^{-14}	4.700×10^{-14}
0.02	2.277×10^{-13}	2.208×10^{-13}	2.371×10^{-13}
0.03	5.796×10^{-12}	5.621×10^{-12}	6.035×10^{-12}
0.03	6.809×10^{-11}	6.605×10^{-11}	7.088×10^{-11}
0.04	2.443×10^{-9}	2.371×10^{-9}	2.541×10^{-9}
0.05	3.088×10^{-8}	2.998×10^{-8}	3.212×10^{-8}
0.06	2.125×10^{-7}	2.063×10^{-7}	2.210×10^{-7}
0.07	9.868×10^{-7}	9.584×10^{-7}	1.026×10^{-6}
0.08	3.490×10^{-6}	3.391×10^{-6}	3.628×10^{-6}
0.09	1.013×10^{-5}	9.841×10^{-6}	1.052×10^{-5}
0.10	2.528×10^{-5}	2.458×10^{-5}	2.626×10^{-5}
0.11	5.616×10^{-5}	5.460×10^{-5}	5.833×10^{-5}
0.12	1.136×10^{-4}	1.105×10^{-4}	1.180×10^{-4}
0.13	2.131×10^{-4}	2.074×10^{-4}	2.213×10^{-4}
0.14	3.754×10^{-4}	3.653×10^{-4}	3.896×10^{-4}
0.15	6.272×10^{-4}	6.104×10^{-4}	6.508×10^{-4}
0.16	1.002×10^{-3}	9.753×10^{-4}	1.039×10^{-3}
0.18	2.290×10^{-3}	2.230×10^{-3}	2.375×10^{-3}
0.20	4.654×10^{-3}	4.532×10^{-3}	4.825×10^{-3}
0.25	1.910×10^{-2}	1.862×10^{-2}	1.979×10^{-2}
0.30	5.558×10^{-2}	5.421×10^{-2}	5.755×10^{-2}
0.35	1.295×10^{-1}	1.264×10^{-1}	1.340×10^{-1}
0.40	2.590×10^{-1}	2.529×10^{-1}	2.678×10^{-1}
0.45	4.631×10^{-1}	4.524×10^{-1}	4.787×10^{-1}
0.50	7.614×10^{-1}	7.440×10^{-1}	7.866×10^{-1}
0.60	1.714×10^{0}	1.676×10^{0}	1.769×10^{0}
0.70	3.251×10^{0}	3.179×10^{0}	3.353×10^{0}
0.80	5.478×10^{0}	5.359×10^{0}	5.647×10^{0}
0.90	8.475×10^{0}	8.293×10^{0}	8.732×10^{0}
1.00	1.230×10^{1}	1.203×10^{1}	1.266×10^{1}
1.25	2.564×10^{1}	2.510×10^{1}	2.637×10^{1}
1.50	4.444×10^{1}	4.350×10^{1}	4.567×10^{1}
1.75	6.852×10^{1}	6.705×10^{1}	7.035×10^{1}
2.0	9.753×10^{1}	9.544×10^{1}	1.001×10^{2}
2.5	1.689×10^{2}	1.653×10^{2}	1.731×10^{2}
3.0	2.559×10^{2}	2.503×10^{2}	2.621×10^{2}
3.5	3.564×10^{2}	3.487×10^{2}	3.648×10^{2}
4	4.689×10^{2}	4.586×10^{2}	4.797×10^{2}

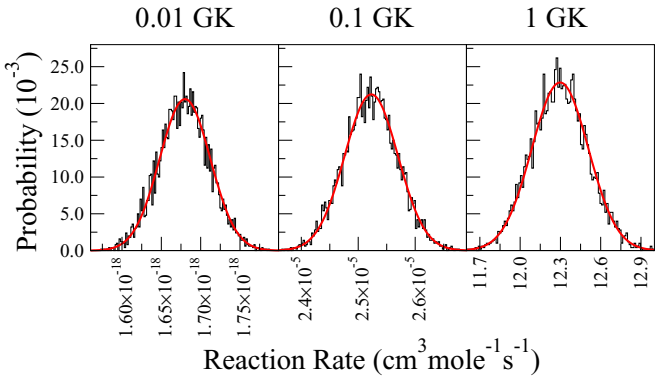

FIG. 10. (Color online) Example probability density functions of the reaction rate of ^{3}He$(\alpha,\gamma)^7$Be at representative temperatures of $T = 0.01$, 0.1, and 1 GK. The red solid line is a Gaussian fit to the PDF for comparison. The uncertainties are calculated by taking the quantiles at 16% and 84%. The central value of the reaction rate is taken at the 50% quantile.

to a very high degree of accuracy and precision. By combining the experimental results of the recent measurements, all of which are in excellent agreement, the uncertainty on the reaction rate can be reduced. An R-matrix model, which gives a good description of the experimental cross sections when both external and internal contributions are included, has been subjected to a more complete uncertainty analysis. The result is a reduction in the uncertainty of $S(0)$ from the value of $S(0) = 0.56 \pm 0.02(\text{expt}) \pm 0.02(\text{theor})$ keV b given in Ref. [1] to $S(0) = 0.542 \pm 0.011(\text{MC fit}) \pm 0.006(\text{model})^{+0.019}_{-0.011}(\text{phase shifts})$ keV b. The resulting reaction rate reduces the uncertainty of the ^{7}Be and ^{8}B solar neutrino fluxes from 6.2% and 12.5% to $+5.8/-5.4$% and $+12.3/-12.2$% respectively. Despite this reduction, the ^{3}He$(\alpha,\gamma)^7$Be reaction rate remains the largest contribution to the uncertainty in the SSM model for predicting the flux of ^{7}Be neutrinos. Moreover, the central value is about 4% lower than the one used in Ref. [56], therefore the ^{7}Be and ^{8}B fluxes will be reduced by a similar amount. This lower central value may have an effect in the assessment of the SSM.

As an outlook for further experiments, three investigations seem to be the most pertinent. First, the R-matrix model should be further tested be expanding measurements to higher energies. Above the proton separation energy several broad resonances are known to exist [36] and these may make significant contributions to the capture cross section. Further, these measurements may shed light on conflicting measurements of the ^{6}Li$(p,\gamma)^7$Be cross section (see, e.g., Refs. [57,58]). Second, there is overlap between the different experimental studies across the entire energy range except for the LUNA data [15]. These are the lowest energy measurements but do not themselves extend to higher energy. While the R-matrix fit seems to naturally extend through these data points, their connection to higher energy data should be confirmed. Therefore, a new study, extending the previous underground measurements towards lower energies, spanning a wide energy range seems mandatory. Such an experiment should have a high statistical significance over the entire energy range in order to test the calculated energy dependence. Last, the elastic scattering cross section should be confirmed. In particular, a new study covering a wide angular range at energies similar to the capture data with detailed uncertainty estimates would better constrain the low-energy capture S factor and the underlying physical parameters.

ACKNOWLEDGMENTS

The authors would like to express their thanks to R. E. Azuma for his many years of dedication to the nuclear astrophysics community. Without his efforts in building the AZURE code and the AZURE Collaboration this work, and many others, would not have been possible. This work was funded by the National Science Foundation through Grant No. PHY-1068192, and the Joint Institute for Nuclear Astrophysics through Grant No. PHY08-22648.

[1] E. G. Adelberger, A. García, R. G. H. Robertson, K. A. Snover, A. B. Balantekin, K. Heeger, M. J. Ramsey-Musolf, D. Bemmerer, A. Junghans, C. A. Bertulani *et al.*, Rev. Mod. Phys. **83**, 195 (2011).

[2] G. Bellini, J. Benziger, D. Bick, S. Bonetti, G. Bonfini, M. Buizza Avanzini, B. Caccianiga, L. Cadonati, F. Calaprice, C. Carraro *et al.* (Borexino Collaboration), Phys. Rev. Lett. **107**, 141302 (2011).

[3] B. Aharmim, S. N. Ahmed, A. E. Anthony, N. Barros, E. W. Beier, A. Bellerive, B. Beltran, M. Bergevin, S. D. Biller, K. Boudjemline *et al.* (SNO Collaboration), Phys. Rev. C **81**, 055504 (2010).

[4] A. Serenelli, C. Peña-Garay, and W. C. Haxton, Phys. Rev. D **87**, 043001 (2013).

[5] P. D. Parker and R. W. Kavanagh, Phys. Rev. **131**, 2578 (1963).

[6] H. D. Holmgren and R. L. Johnston, Phys. Rev. **113**, 1556 (1959).

[7] H. Kräwinkel, H. Becker, L. Buchmann, J. Görres, K. Kettner, W. Kieser, R. Santo, P. Schmalbrock, H. Trautvetter, A. Vlieks *et al.*, Z. Phys. A **304**, 307 (1982).

[8] R. G. H. Robertson, P. Dyer, T. J. Bowles, R. E. Brown, N. Jarmie, C. J. Maggiore, and S. M. Austin, Phys. Rev. C **27**, 11 (1983).

[9] H. Volk, H. Kräwinkel, R. Santo, and L. Wallek, Z. Phys. A **310**, 91 (1983).

[10] T. Alexander, G. Ball, W. Lennard, H. Geissel, and H.-B. Mak, Nucl. Phys. **427**, 526 (1984).

[11] J. Osborne, C. Barnes, R. Kavanagh, R. Kremer, G. Mathews, J. Zyskind, P. Parker, and A. Howard, Nucl. Phys. **419**, 115 (1984).

[12] M. Hilgemeier, H. Becker, C. Rolfs, H. Trautvetter, and J. Hammer, Z. Phys. A **329**, 243 (1988).

[13] A. Kontos, E. Uberseder, R. deBoer, J. Görres, C. Akers, A. Best, M. Couder, and M. Wiescher, Phys. Rev. C **87**, 065804 (2013).

[14] B. S. Nara Singh, M. Hass, Y. Nir-El, and G. Haquin, Phys. Rev. Lett. **93**, 262503 (2004).
[15] H. Costantini, D. Bemmerer, F. Confortola, A. Formicola, G. Gyürky, P. Bezzon, R. Bonetti, C. Broggini, P. Corvisiero, Z. Elekes *et al.*, Nucl. Phys. **814**, 144 (2008).
[16] T. A. D. Brown, C. Bordeanu, K. A. Snover, D. W. Storm, D. Melconian, A. L. Sallaska, S. K. L. Sjue, and S. Triambak, Phys. Rev. C **76**, 055801 (2007).
[17] A. Di Leva, L. Gialanella, R. Kunz, D. Rogalla, D. Schürmann, F. Strieder, M. De Cesare, N. De Cesare, A. D'Onofrio, Z. Fülöp *et al.*, Phys. Rev. Lett. **102**, 232502 (2009).
[18] M. Carmona-Gallardo, B. S. Nara Singh, M. J. G. Borge, J. A. Briz, M. Cubero, B. R. Fulton, H. Fynbo, N. Gordillo, M. Hass, G. Haquin *et al.*, Phys. Rev. C **86**, 032801 (2012).
[19] G. Gyürky, F. Confortola, H. Costantini, A. Formicola, D. Bemmerer, R. Bonetti, C. Broggini, P. Corvisiero, Z. Elekes, Z. Fülöp *et al.* (LUNA Collaboration), Phys. Rev. C **75**, 035805 (2007).
[20] F. Confortola, D. Bemmerer, H. Costantini, A. Formicola, G. Gyürky, P. Bezzon, R. Bonetti, C. Broggini, P. Corvisiero, Z. Elekes *et al.* (LUNA Collaboration), Phys. Rev. C **75**, 065803 (2007).
[21] C. Bordeanu, G. Gyürky, Z. Halász, T. Szücs, G. Kiss, Z. Elekes, J. Farkas, Z. Fülöp, and E. Somorjai, Nucl. Phys. **908**, 1 (2013).
[22] T. A. Tombrello and P. D. Parker, Phys. Rev. **131**, 2582 (1963).
[23] T. Neff, Phys. Rev. Lett. **106**, 042502 (2011).
[24] T. Kajino, Nucl. Phys. **460**, 559 (1986).
[25] K. M. Nollett, Phys. Rev. C **63**, 054002 (2001).
[26] A. M. Lane and R. G. Thomas, Rev. Mod. Phys. **30**, 257 (1958).
[27] R. Christy and I. Duck, Nucl. Phys. **24**, 89 (1961).
[28] F. Barker and T. Kajino, Austral. J. Phys. **44**, 369 (1991).
[29] C. Angulo and P. Descouvemont, Nucl. Phys. **690**, 755 (2001).
[30] A. Lane and J. Lynn, Nucl. Phys. **17**, 563 (1960).
[31] R. E. Azuma, E. Uberseder, E. C. Simpson, C. R. Brune, H. Costantini, R. J. de Boer, J. Görres, M. Heil, P. J. LeBlanc, C. Ugalde *et al.*, Phys. Rev. C **81**, 045805 (2010).
[32] E. Uberseder and R. J. deBoer (unpublished), azure.nd.edu.
[33] C. R. Brune, Phys. Rev. C **66**, 044611 (2002).
[34] A. Barnard, C. Jones, and G. Phillips, Nucl. Phys. **50**, 629 (1964).
[35] C. Rolfs, Nucl. Phys. **217**, 29 (1973).
[36] D. Tilley, C. Cheves, J. Godwin, G. Hale, H. Hofmann, J. Kelley, C. Sheu, and H. Weller, Nucl. Phys. **708**, 3 (2002).
[37] R. J. Spiger and T. A. Tombrello, Phys. Rev. **163**, 964 (1967).
[38] J. A. McCray, Phys. Rev. **130**, 2034 (1963).
[39] P. Tischhauser, R. E. Azuma, L. Buchmann, R. Detwiler, U. Giesen, J. Görres, M. Heil, J. Hinnefeld, F. Käppeler, J. J. Kolata *et al.*, Phys. Rev. Lett. **88**, 072501 (2002).
[40] G. D'Agostini, Nucl. Instrum. Methods. Phys. Res. Sect. A **346**, 306 (1994).
[41] R. H. Cyburt and B. Davids, Phys. Rev. C **78**, 064614 (2008).
[42] W. Press, S. Teukolsky, W. Vetterling, and B. Flannery, *Numerical Recipies: The Art of Scientific Computing* 3rd. ed. (Cambridge University Press, New York, 2007).
[43] G. Cowan, *Statistical Data Analysis* (Clarendon, Oxford, 2007).
[44] L. Gialanella, D. Rogalla, F. Strieder, S. Theis, G. Gyürky, C. Agodi, R. Alba, M. Aliotta, L. Campajola, A. Del Zoppo *et al.*, Eur. Phys. J. A **11**, 357 (2001).
[45] D. Schürmann, L. Gialanella, R. Kunz, and F. Strieder, Phys. Lett. B **711**, 35 (2012).
[46] P. Mohr, H. Abele, R. Zwiebel, G. Staudt, H. Krauss, H. Oberhummer, A. Denker, J. W. Hammer, and G. Wolf, Phys. Rev. C **48**, 1420 (1993).
[47] P. D. Miller and G. C. Phillips, Phys. Rev. **112**, 2048 (1958).
[48] T. A. Tombrello and P. D. Parker, Phys. Rev. **130**, 1112 (1963).
[49] M. Ivanovich, P. Young, and G. Ohlsen, Nucl. Phys. **110**, 441 (1968).
[50] L. Chuang, Nucl. Phys. **174**, 399 (1971).
[51] W. Boykin, S. Baker, and D. Hardy, Nucl. Phys. **195**, 241 (1972).
[52] D. Hardy, R. Spiger, S. Baker, Y. Chen, and T. Tomberllo, Nucl. Phys. **195**, 250 (1972).
[53] V. Zerkin, http://www-nds.iaea.org/exfor/exfor.htm
[54] P. Mohr (private communication).
[55] W. A. Fowler, G. R. Caughlan, and B. A. Zimmerman, Annu. Rev. Astron. Astrophys. **5**, 525 (1967).
[56] A. M. Serenelli, W. C. Haxton, and C. Peña-Garay, Astrophys. J. **743**, 24 (2011).
[57] R. M. Prior, M. C. Spraker, A. M. Amthor, K. J. Keeter, S. O. Nelson, A. Sabourov, K. Sabourov, A. Tonchev, M. Ahmed, J. H. Kelley *et al.*, Phys. Rev. C **70**, 055801 (2004).
[58] J. He, S. Chen, C. Rolfs, S. Xu, J. Hu, X. Ma, M. Wiescher, R. deBoer, T. Kajino, M. Kusakabe *et al.*, Phys. Lett. B **725**, 287 (2013).